Renewable Energy
January 2019, Volume 130, Pages 245-255
http://dx.doi.org/10.1016/j.renene.2018.06.049
http://archimer.ifremer.fr/doc/00445/55631/

Analytical linear modelization of a buckled undulating membrane tidal energy converter

Träsch Martin [1, 2, 3, *], Déporte Astrid [1], Delacroix Sylvain [1], Germain Gregory [2], Drevet Jean-Baptiste [1]

[1] Eel Energy, 42 Rue Monge, 75005 Paris, France
[2] Ifremer, Marine Structure Laboratory, 150 Quai Gambetta, 62200 Boulogne sur Mer, France
[3] Ademe, 20 Avenue du Gresille, 49004 Angers, France

* Corresponding author : Martin Träsch, email address : mtrasch@eel-energy.fr

Abstract :

This paper presents an analytical linear model developed to study the behaviour of a buckled membrane tidal energy converter. The Euler beam theory and the elongated body theory are used for the fluid structure interaction formulation. The effect of electromechanical converters used to convert the undulating motion into electrical energy is reproduced by adding a term equivalent to viscous material damping.

The influence of compression force, flaps and hanging conditions is studied, as well as the effects of simulated power take-off through internal damping. The system's behaviour is characterized by undulating mode, critical flow velocity, motion frequency and amplitude.

The model shows good agreement in terms of frequency and satisfactory results for the amplitude compared to experimental data. The linear assumptions were validated on fluid and structure models as a good start for a first analytical model describing the system's physic. The obtained results confirmed the benefits of initial stress and optimized damping to the tidal converter for energy harnessing.

Highlights

► The behaviour of an undulating membrane tidal energy convertor has been modelized. ► The model is linearized to enable light computation. ► Results of frequency, trajectory and hydrodynamic forces fit the experiments. ► Optimization of the tidal energy collected is discussed.

Keywords : Marine renewable energy, Tidal energy converter, Power take-off, Fluid-structure interaction, Slender body theory

Nomenclature

A	Dimensional maximum amplitude
$[\tilde{A}]$	Eigenvector of the equation system
a	Non-dimensional amplitude calibration
$a_{1..4}$	Coefficient for shape function
$\tilde{a_i}$	Modal relative amplitude
$[C]$	Damping matrix
C_d	Drag coefficient
D	Damping coefficient for material viscosity
D'	Damping coefficient for Power Take-Off
d	Cable length
E	Young's modulus
$\mathcal{F}_{flap}$	Flap localized load
F_d	Drag force
F_{flap}	Flap force coefficient
F_l	Lift force
f_d	Non-dimensional drag force
f_{flap}	Non-dimensional flap force coefficient
f_l	Non-dimensional lift force
I	Quadratic moment
$[\mathcal{I}]$	Identity matrix
i	Imaginary number
$()_i, ()_j$	Modal indices
$[K]$	Stiffness matrix
L	Total length
L_0	Membrane length
L_a	Membrane width
$[M]$	Mass matrix
m_f	Fluid linear added mass
m_s	Solid linear mass
N	Number of modes used in calculation

P	Harvested power
p	Non-dimensional collected power
Q	Linear external load
q_j	Non-dimensional time function
$[R]$	Calculus matrix
S	Frontal area
s	Curvilinear coordinate along the beam
T	Cable compression force
$\mathcal{T}$	Period
t	Time
U	Upstream flow speed
U_c	Critical velocity
u	Non-dimensional flow speed
x	Horizontal position
y	Vertical position
w	Fluid velocity orthogonal to the body
β	Mass ratio
Γ	Non-dimensional cable compression force
γ_i	Eigenvalue of the system
ΔP	Pressure difference along the beam
δ_j^i	Kronecker delta
η	Non-dimensional beam deflection
θ	Local angle with horizon
ι	Non-dimensional cable length
λ	Wave number
ξ	Non-dimensional curvilinear coordinate
ρ_f	Fluid volumic mass
ρ_s	Solid volumic mass
σ_i	Coefficient for shape function
τ	Non-dimensional time
ϕ_i	Non-dimensional shape function
ω_i	Non-dimensional complex frequency

1. Introduction

In these times of energy transition, the idea of using the tidal power of oceans as a renewable energy source arises again. This source has many advantages (Tecnomare (1996)) and a lot of research has been done to find the best way to gather it (Boye et al. (2013)). The corresponding field of research is mainly aimed on turbine-based technologies (Day (2015)) but several other systems have been suggested, based on flow-induced flutter. Various tactics are being adopted to capture energy from fluid through undulating motion, based on vortex-induced vibration in cables (Grouthier et al. (2014), Lee and Bernitsas (2011)), oscillating foils (Kinsey et al. (2011), Xiao and Zhu (2014)) or flexible membranes either distorted by vortex shedding downstream bluff bodies (Shi et al. (2013), Taylor et al. (2001)) or set in motion by axial flow (Doare and Michelin (2011)).

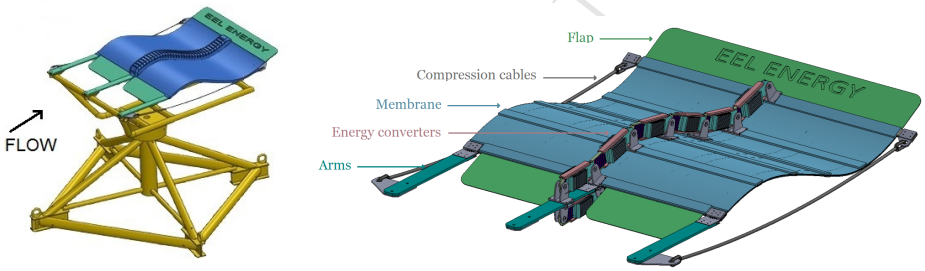

Figure 1: CAD representations of an undulating tidal energy converter

The analytical model presented in this paper is developed to model the behaviour of the undulating tidal energy converter (Fig. 1, Deporte et al. (2015)). It is equivalent to a compressed membrane undulating in axial flow. The membrane is hung by three semi-rigid arms that allow small motion freedom at its upstream extremity. Initial stress is applied to the membrane by cables linking both extremities. They are shorter than the membrane and buckle it. This enables to give an initial shape presenting a larger frontal area to the fluid and enabling the system to be put in motion at a slow flow speed. When operating, the membrane undulates, activating the electromechanical converters distributed along the main center line of the structure. We can observe a propagating wave in the current direction which has a lower celerity than the fluid velocity. This technology is in development and proposes an alternative for classical tidal turbines at low current speed (1-3m/s)(J-B. Drevet (2016)).

Many publications propose analytical model to deal with an elastic plate immersed in an axial uniform flow. We can class these analytical models according to the way they express the fluid loads. Among all formulations, (Huang (1995), Kornecki et al. (1976) and Watanabe et al. (2001)) use the Theodorsen formulation to take into account the vortex circulation around the plate. In continuity, the structure boundaries can be divided into small panels by the use of the panel method (Tang (2007)) to estimate more precisely lift and pressure loads. Another approach consists of imposing continuity of the pressure everywhere except across the plate and of solving the pressure distribution into the Fourier space (Eloy et al. (2007), Guo and Paidoussis (2000)). When the elongated body theory is used, like in (Coene (1988), Lighthill (1960), Païdoussis (1998) and Yadakin et al. (2001)), the potential flow is regarded as the sum of the flow around the structure at rest and the flow disturbed by the displacement of a small body section. The solid motion is in most cases described by an Euler-Bernoulli beam theory.

These models are validated by several experiments on flexible plate or filament in axial flow with various materials (in term of mass and rigidity), characteristic lengths and fluid velocities (Lemaitre et al. (2005), Watanabe et al. (2002), Watanabe et al. (2001)). Most of the cited models are 2D according to the experimental behaviour, but some of them have shown the influence of the aspect ratio (Doare et al. (2011), Eloy et al. (2007)). These models also highlight the influence of mass ratio, rigidity, flow speed and induced tension into the beam. However, the range of parameters used in the works described above are different from our prototype characteristics due to differences in application (paper flutter, swimming fish, pipe conveyed fluid).

The power take-off impact on flexible plate is studied in Doare and Michelin (2011), Pineirua et al. (2015), Singh et al. (2012b), and Tang (2007) with piezoelectric devices. They investigate the intensity and the location of piezoelectric energy converters, but applied to smaller scale devices in comparison.

A special feature of this structure is pre-stress imposed by cables. Many authors take into account an induced tension due to bending (Argentina and Mahadevan (2005), Eloy et al. (2011), Moretti (2003), Shelley et al. (2005)). A pre-tension has been introduced in Coene (1988) and Morris-Thomas and Steen (2009) but in the opposite direction to ours, to stretch the flag. The most representative model is Dowell's model (Dowell (1982)), it represents a buckled plate submitted to a fluid flow. The tension is expressed as a sum of the tension forcing the buckling and the one due to bending.

This paper presents an analytical linear model developed to study the behaviour of a buckled undulating membrane tidal energy converter. The model aims to describe the membrane motion with a simplified formulation. The Euler beam theory and the elongated body theory are used for the fluid structure interaction formulation. The effect of electromechanical converters used to convert the undulating motion into electrical energy is simulated by adding a term equivalent to viscous material damping. It will lead to a better understanding of the influence of main parameters on the system motion. It will also give an expression of the power collected.

In the following, the hypotheses leading to the formulation of the physical modelling are first presented. The system is solved as an eigenvalue problem to find frequency and critical velocity and an approximated equation is used to determine the undulation's amplitude. The model is then compared with experimental data without power take-off. In section 4, the influence of the compression cables on the system is studied. In the last part, we extrapolate the effect of the converters damping coefficient as a simulation of power take-off and assess some power collecting strategies.

2. Analytical model

To model the undulating tidal energy converter, an inextensible membrane (Eq. 1) with small deflections is considered submitted to lateral loads. These hypotheses lead to the Euler-Bernouilli dynamic beam equation (Eq. 2) to describe the system, where m_s is the linear beam mass, EI is the flexural rigidity and $Q(s,t)$ is the external linear load. Gravity and buoyancy are neglected taking into account the very small difference between the membrane density and the water density. The membrane stiffness in the direction transverve to the flow is higher than in the longitudinal one, making the transverse motion very small in comparison to the axial one. That is why three-dimensional effects are neglected to simplify the problem. These hypotheses are often used in literature to describe beams or cantilevered plates motion (see for example: Alben (2008), Eloy et al. (2007), Howell et al. (2008), Morris-Thomas and Steen (2009), Shelley and Zhang (2011)).

$$(\frac{\partial x}{\partial s})^2 + (\frac{\partial y}{\partial s})^2 = 1 \tag{1}$$

$$\frac{\partial^2}{\partial s^2}(EI\frac{\partial^2 y}{\partial s^2}) = -m_s\frac{\partial^2 y}{\partial t^2} + Q(s,t) \tag{2}$$

The flow is considered incompressible, potential and non-viscous. With the assumption that the length of the beam is much greater than its width and thickness, the elongated-body theory can be used (Lighthill (1960)).

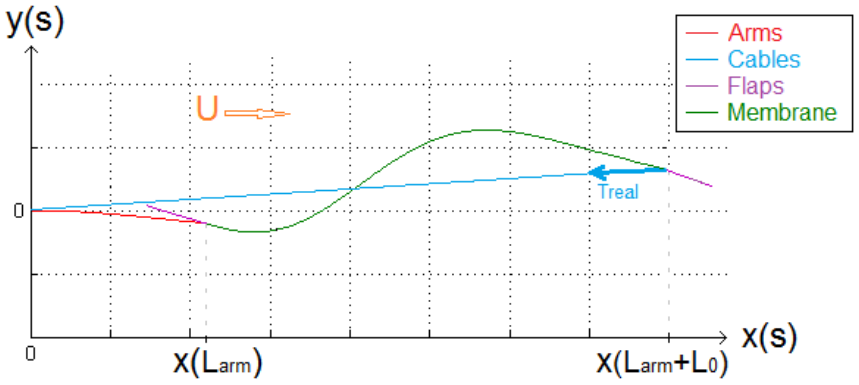

Figure 2: Sketch of the undulating membrane in two dimension

A classical result of the elongated-body theory (Lighthill (1960)) is Eq. 3 where $m_f = \rho_f \frac{\lambda}{\pi}$ is the approximation of added mass for wide flags (Moretti (2004)) and $w(s,t)$ the fluid velocity orthogonal to the solid body.

$$\Delta P(s,t) = m_f(\frac{\partial}{\partial t} + U\frac{\partial}{\partial s})w(s,t) \tag{3}$$

This leads to Eq. 4 for the pressure difference formulation.

$$\Delta P = m_f(\frac{\partial}{\partial t} + U\frac{\partial}{\partial s})^2 y \tag{4}$$

Combining Eq. 2 and Eq. 4, we get to Eq. 5 describing the dynamics of a flexible beam interacting with axial flow.

$$EI\frac{\partial^4 y}{\partial s^4} + m_s\frac{\partial^2 y}{\partial t^2} = -[m_f U^2\frac{\partial^2 y}{\partial s^2} + 2m_f U\frac{\partial^2 y}{\partial s \partial t} + m_f\frac{\partial^2 y}{\partial t^2}] \tag{5}$$

However, this formulation is not adequate to reproduce the undulating tidal converters motion. The aspect ratio is close to one which is not suitable for the theory used here (Eloy et al. (2007)). Furthermore the small displacement assumption is exaggerated above critical speed as membrane amplitude is of the order of L/2. Although these assumptions (aspect ratio,

small displacement) are different from our model, the results shown later on prove that this model can still work on our concept. However if we consider large displacement we would need to develop non-linear equation and greatly complexify the model (Alben (2008)). These two limits will be the object of further improvements of the model.

It is also necessary to add several parameters to get closer to the specificity of the system. One of the main differences with other models is that the membrane is buckled and compressed by lateral cables (Fig. 1 and Fig. 2). We also consider the arms that hang the membrane and the flaps at the upstream and downstream ends.

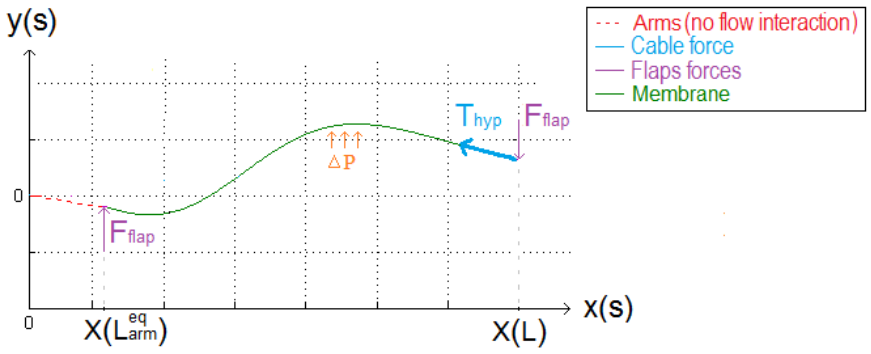

Figure 3: Sketch of the linear model used to model the undulating membrane

To take the buckling into account, we consider the same formulation as Morris-Thomas and Steen (2009) with an opposite sign of the tension (Dowell (1982)). This formulation is equivalent to a force tangent to the membrane's downstream extremity : T_{hyp} on Fig. 3, which is close to T_{real} in the small angle hypothesis. Moreover, we suppose that this force is constant, while in fact it oscillates around a mean value depending on the membranes shape and position (Träsch et al (2017)). We decomposed the compression force in two components: one responsible for buckling the membrane, the other one caused by fluid pressure drag resultant. The buckling component is assumed equal to the Euler critical load for a clamped/free beam, thus with an effective length factor of 2, with L the total membrane length. The drag component C_d is adjusted to fit the experiments (Eq. 6).

$$T_{Total} = T_{buckling} + T_{drag} = \frac{\pi^2 \times EI}{(2L)^2} + \frac{1}{2} C_d \rho_f S U^2 \tag{6}$$

The arms are semi-rigid parts that link the membrane to its support. They are modelled by an additional membrane length with the same properties as the membrane. We calculate the membrane length that would have a stiffness equivalent to the arm and we add it to membrane length L_0 to get the total modelled membrane length L (Eq. 7). Here, $E_{arms}I_{arms} = 11.04EI$ The equivalent length corresponding to the arms does not interact with the fluid. This assumption gives a good representation on deflection at the membrane's upstream extremity, but accentuates artificially the slope.

$$L = L_0 + L_{arms}^{eq} = L_0 + L_{arms}\sqrt[3]{\frac{EI}{E_{arms}I_{arms}}} \tag{7}$$

The flaps are rigid extension in the continuities of the membrane extremities. They enhance lift at extremities and increase motion amplitude. Their effects are assumed equivalent to local vertical forces equal to the lift force generated by an uniform flow on an inclined plate of angle $\theta_{s_{flap}}$ and of the same area as the flap. Here s_{flap} is the position of the flaps on the membrane. In our case it is equivalent to $s = L_{arms}^{eq.}$ for the upsteram flap and $s = L$ for the downstream flap. We have then a localized load $\mathcal{F}_{flap}$ proportional to local slope as described by Eq. 8, where δ_i^j is Kronecker's delta.

$$\mathcal{F}_{flap} = F_{flaps}\theta(s,t)\delta_s^{s_{flap}} = \pi\rho_f L_{flap}U^2\frac{\partial y}{\partial s}\delta_s^{s_{flap}} \tag{8}$$

We choose to take into account the material damping through the formulation of a visco-elastic Kelvin-Voigt material with D the apparent viscosity. The Power Take-Off (PTO) system is also represented as an additional term of viscous material damping (Eq. 9), as has already been modelled by Singh et al. (2012b) for the approximation of the effect of piezoelectric films. Here D' is the parameter simulating the power conversion, leading to collected power evaluation.

$$F_{viscoelastic} = (D + D')\frac{\partial^5 y}{\partial t \partial s^4} \tag{9}$$

All the previous hypotheses permit to represent the undulating membrane behaviour by the following variational formulation:

$$EI\frac{\partial^4 y}{\partial s^4} + (m_f U^2 + T)\frac{\partial^2 y}{\partial s^2} + F_{flap}\frac{\partial y}{\partial s}\delta_s^{s_{flap}} + (D+D')\frac{\partial^5 y}{\partial s^4 \partial t} + 2m_f U\frac{\partial^2 y}{\partial s \partial t} + (m_s + m_f)\frac{\partial^2 y}{\partial t^2} = 0 \tag{10}$$

3. Resolution and behavioural study

In this section the variational formulation of the system is written in its non-dimensionalized form. It is then solved by Galerkin decomposition, assuming cantilever natural shape modes and a periodic motion. An eigenvalue solution leads to the frequency and stability results whereas a different equation using the cable length is developed to determine the motion amplitude. Forces are also expressed by the integration of pressure load on the structure. These parameters are then compared with experimental data obtained with a 1:20 scale prototype described in Deporte et al. (2015).

3.1. Resolution steps

In order to simplify the problem and allow a better comparison with the existing literature, Eq. 10 is written in its non-dimensionalized form. The non-dimensional parameters used here are the following:

$\beta = \frac{m_f}{m_f+m_s}$	Mass ratio
$u = UL\sqrt{\frac{m_f}{EI}}$	Non-dimensional speed
$\mu = \frac{D+D'}{L^2\sqrt{EI(m_f+m_s)}}$	Non-dimensional damping
$\Gamma = \frac{L^2T}{EI}$	Non-dimensional cable compression force
$f_{flap} = \frac{F_{flap}L^3}{EI}$	Non-dimensional flap force coefficient
$\eta = \frac{y}{L}$	Non-dimensional beam deflection
$\xi = \frac{s}{L}$	Non-dimensional curvilinear coordinates
$\tau = \frac{t}{L^2}\sqrt{\frac{EI}{m_f+m_s}}$	Non-dimensional time

This brings to the following non-dimensional equation, where the following notations are used: $()' = \frac{\partial}{\partial \xi}$ and $\dot{()} = \frac{\partial}{\partial \tau}$:

$$\eta'''' + (u^2 + \Gamma)\eta'' + f_{flap}\eta'\delta_{\xi}^{\xi_{flap}} + \mu\dot{\eta}'''' + 2\beta^{1/2}u\dot{\eta}' + \ddot{\eta} = 0 \qquad (11)$$

This system is solved with a particular solution, considering a sum of periodic motions (Eq. 12, 13 and 14) and a constant wavelength (Païdoussis (1998)). The Galerkin solution of variable separation is then applied:

$$\eta(\xi,\tau) = Re[\Sigma_{j=1}^{N}\phi_j(\xi)q_j(\tau)] \tag{12}$$

with:

$$q_j(\tau) = \tilde{a_j}e^{i\omega_j\tau} \tag{13}$$

and:

$$\phi_j(\xi) = a_1\cosh(\lambda_j\xi) + a_2\sinh(\lambda_j\xi) + a_3\cos(\lambda_j\xi) + a_4\sin(\lambda_j\xi) \tag{14}$$

Coefficients a_1 to a_4 are found through the beam boundary conditions. We consider here a cantilever beam (clamped-free), such as:

$$\forall t, \begin{cases} \phi_j(\xi=0) = 0 \\ \phi_j'(\xi=0) = 0 \\ \phi_j''(\xi=1) = 0 \\ \phi_j'''(\xi=1) = 0 \end{cases}$$

This brings us to the following shape functions, visible on Fig. 4 for the first four natural modes in vacuum of a cantilever beam:

$$\phi_j(\xi) = a[\cosh(\lambda_j\xi) - \cos(\lambda_j\xi) - \sigma_j(\sinh(\lambda_j\xi) - \sin(\lambda_j\xi))]; \tag{15}$$

where a is a constant and σ_j is a coefficient depending on the mode:

$$\sigma_j = \frac{\sinh(\lambda_j) - \sin(\lambda_j)}{\cosh(\lambda_j) + \cos(\lambda_j)} \tag{16}$$

λ_j is part of the natural wavenumbers of cantilever beams:

$$\lambda_j \in [1.876, 4.695, 7.855, 10.996, 11.138, 17.279, ...] \tag{17}$$

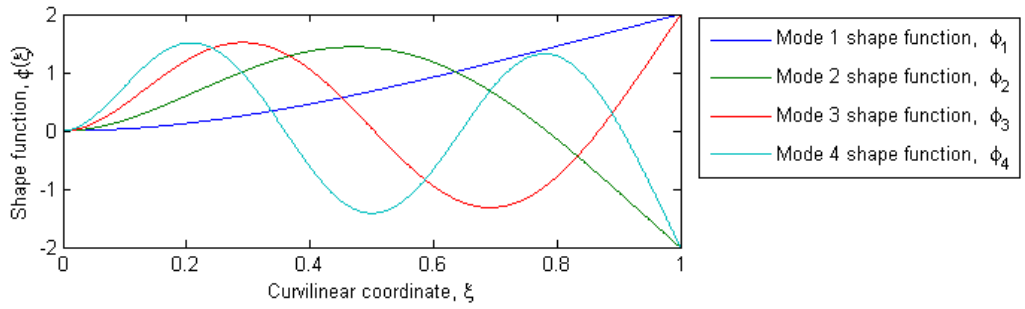

Figure 4: First four natural modes of a cantilevered beam

In order to obtain an ordinary differential equation of order 2, we combine Eq. 11 with Eq. 12, Eq. 13 and Eq. 15, then multiply by ϕ_i, and integrate on interval $[0, 1]$, such as done by Païdoussis (1998). The system to solve is then Eq. 18 for $j = 1$ to N. Here, N=6 modes.

$$[M]\ddot{q}_j + [C]\dot{q}_j + [K]q_j = 0 \tag{18}$$

Mass matrix [M], damping matrix [C] and stiffness matrix [K] are defined by:

- $M_{ij} = d_{ij}$
- $C_{ij} = \mu\lambda_j^4\delta_{ij} + 2\beta^{1/2}uc_{ij}$
- $K_{ij} = \lambda_j^4\delta_{ij} + (u^2 + \Gamma)b_{ij} + f_{flap}\phi_j'(\xi_{arms}^{eq.})\phi_i(\xi_{arms}^{eq.}) + f_{flap}\phi_j'(1)\phi_i(1)$;

with the coefficients:

- $b_{ij} = \int_{\xi_{arms}^{eq.}}^{1} \phi_j''\phi_i \mathrm{d}\xi$
- $c_{ij} = \int_{\xi_{arms}^{eq.}}^{1} \phi_j'\phi_i \mathrm{d}\xi$
- $d_{ij} = \int_{\xi_{arms}^{eq.}}^{1} \phi_j\phi_i \mathrm{d}\xi$

These coefficients are integrated from $\xi_{arms}^{eq.}$ to 1: we consider here that arms have no mass and no interaction with the fluid flow. The only interaction with the system is through the stiffness term, integrated from 0 to 1.

A particular solution of this system (Eq. 18) is in the form of Eq. 13: $q(\tau) = \tilde{a}e^{\gamma\tau} = \tilde{a}e^{i\omega\tau}$ which is equivalent to consider the following eigenvalue problem :

$$(\gamma[\mathcal{I}] - [R])[\tilde{A}] = 0 \tag{19}$$

Here, $[\mathcal{I}]$ is the identity matrix and $[\tilde{A}]$ is the eigenvector, set within a multiplication factor, composed by the relative amplitude of each mode $\tilde{a_j}$. The following matrix is also defined by:

$$[R] = \begin{bmatrix} -M^{-1}C & -M^{-1}K \\ \mathcal{I} & 0 \end{bmatrix} \tag{20}$$

Eigenfrequencies ω_j are $[R]$ matrix eigenvalues γ_j divided by imaginary number i. Undulation mode is then selected, knowing that unstable modes have negative imaginary part of their eigenfrequencies (i.e. positive real part of their eigenvalue, Païdoussis (1998)).

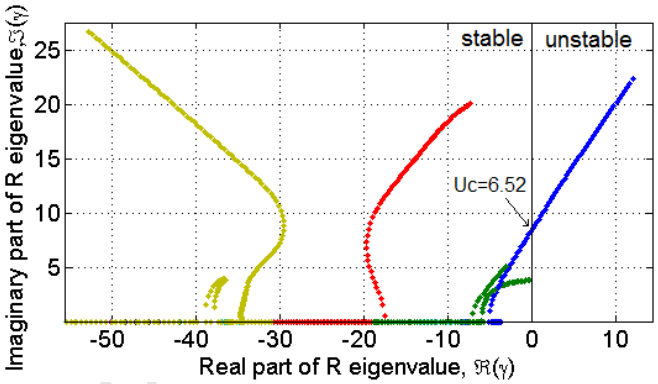

Figure 5: R eigenvalues for $\beta = 0.991$, $\mu = 0.0292$, $2.47 < \Gamma < 42.6$, $0.10 < u < 11.56$. First mode in green, second mode in blue, third mode in red, fourth mode in yellow. Fifth and sixth modes are out of the graph ($\Re(\gamma) < -60$).

Fig. 5 shows the Agrand diagram of the membrane's first modes for different flow speeds. Imaginary part represents the system's frequency and the real part the negative damping. The critical velocity u_c can be found when the real part of the eigenvalue becomes positive, indicating that the system is unstable. In this case it happens for the second mode at $u_c = 6.52$. Real dimensional frequencies are then obtained by taking the real part of ω, multiplying by t/τ and dividing by 2π.

Eigenmodes are set within a constant. Considering only one excited frequency, we can reduce both factors before $\phi(\xi)$ (Eq. 14) and $q(\tau)$ (Eq. 13) to one parameter representing motion amplitude calibration, a. We use the cable length to define this non-dimensional amplitude calibration. The cable length is assumed constant, as it limits the position of the membrane's downstream end to a certain distance d to its fixation. The fixation point is set to be at the origin of the frame $(x(0), y(0)) = (0, 0)$ (Fig. 3), enabling to write Eq. 21:

$$x(L)^2 + y(L)^2 = d^2 \tag{21}$$

The inextensibility equation (Eq. 1) then leads to Eq. 22:

$$x(s) = \int_0^s \sqrt{1 - (\frac{\partial y}{\partial s})^2} ds \tag{22}$$

Eq. 21 and Eq. 22 are combined, and a first order Taylor expansion on the square root is done. Neglecting the 4-order term, and dividing by L^2, we get to Eq. 23, where $\iota = d/L$ is the non-dimensional cable length.

$$1 - \int_0^1 \eta'^2 \mathrm{d}s + \eta_L^2 = \iota^2 \tag{23}$$

From Eq. 12, and considering only one unstable frequency ω, η is expressed as the sum of the complex conjugates:

$$\eta(\xi, \tau) = \frac{a}{2}(\Phi \exp(i\omega\tau) + \bar{\Phi} \exp(-i\omega\tau)) \tag{24}$$

Where $\Phi = \Sigma_{j=1}^{N} \tilde{a_j} \phi_j$, with $\tilde{a_j}$ the (N+j)th element of the eigenvector associated with unstable mode (Eq. 19). Then, we substitute η and separate terms that are constant in time to those that vary. We obtain Eq. 25:

$$1 - \iota^2 = 2(\frac{a}{2})^2 [\int_0^1 |\Phi'|^2 \mathrm{d}s - |\Phi_L|^2] \tag{25}$$

Nondimensional amplitude's formulation is then given by Eq. 26 and $A = \max(\eta \times L) = \max(a \times Re[\Phi(1)] \times L)$ is the dimensional amplitude at the downstream edge.

$$a = 2\sqrt{\frac{1 - \iota^2}{2(\int_0^1 |\Phi'|^2 \mathrm{d}s - |\Phi_1|^2)}} \tag{26}$$

3.2. Comparison with experimental data

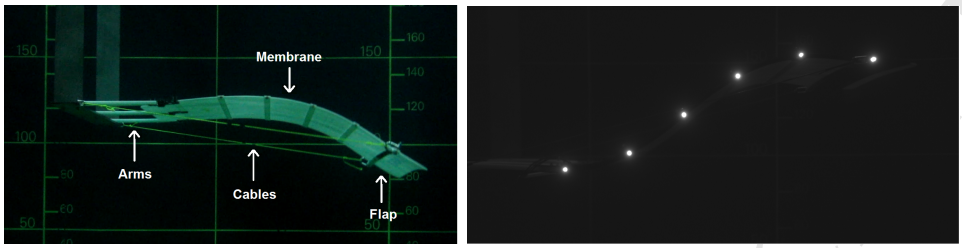

Figure 6: Pictures of the experimental set-up used to validate the analytical model

The experimental set-up used for comparison and validation of this analytical model is the one described in Träsch et al (2017). Trials took place in the flume tank of Ifremer in Boulogne-sur-Mer with a $1/20^{th}$ scale prototype which is about 1 m long, 0.8 m wide and 0.004 m thick. It is made of a POM-C polyacetal membrane of density $\rho = 1600$ kg/m^3 and Young modulus E = 4.2 GPa [Déporte (2015)].

Rigid flaps at upstream and downstream extremities lengthen the membrane by $L_{flap} = 0.15L$ each and enhance its undulation motion. Six $0.025L$-wide carbon-epoxy bars have been added in the transverse direction in order to increase the transverse stiffness and to ensure a two-dimensional motion. They also transmit forces to the converters, that are linked to it by $h_{fix} = 0.044L$-high fixations. Each fixation is separated by $0.2L$ on the membrane and linked to dampers through pivot points.

To keep the structure in the middle of the water column, the membrane is linked to a rigid vertical frame with three flexible arms of rigidity $k_{arm} = 6250$ N/m. The structure is also stressed by cables linking both extremities that keep the membrane bended (Figure 6). The cables are $d = 0.046L$ shorter than the resting distance between their linking points.

The picture on the left of Fig. 6 shows the experimental set-up and the one on the right shows a frame with six luminous targets used for motion tracking. The motion tracking system enables to assess the structures dynamic behaviour and to characterise motion in terms of undulation amplitude and frequency.

Instantaneous deformation resulting from the analytical model and the experiments are plotted on Fig. 8, which enables a qualitative visual comparison indicating that undulations occur on the same mode for both kind of results.

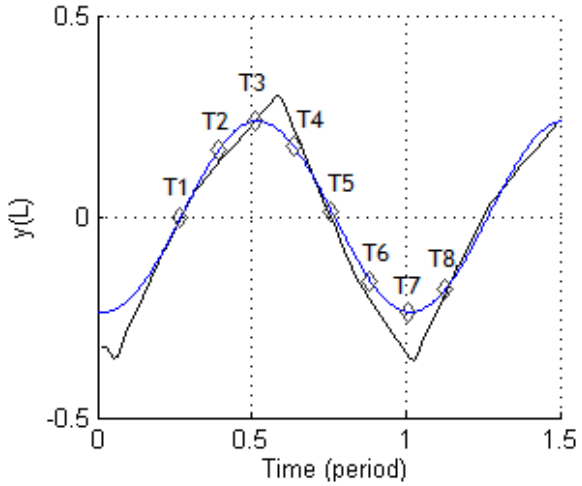

Figure 7: Time variation of downstream end position of analytical model results (blue) and experiment results (black). Times of frames in Fig. 8 are represented as diamonds.

A period is here divided in eight moments, as shown in Fig. 7, with downstream tip rising at $y_L = 0$ as the sarting time. Then, for each moment (eight in a period), a frame of the membrane instantaneous shape is printed from the model.

There is a good agreement between the model and experiments shape results even if a few differences can be noticed. The model underestimates the curvature at the membrane's end. Indeed, the cable is not taken into account as a boundary condition ruling the shape and the cable force direction is constant in regard to downstream end. The membrane's motion during the experiment wasn't perfectly symmetric, with a slower inversion during the rise than during the fall. This difference comes from the effect of gravity and explains the little phase difference we can observe here. The agreement with experiment is overall very good and forms a first validation for the model.

Comparison of frequency between experimental results and the analytical model is shown on the left of Fig. 9. The model gives good results for frequency, with good order of magnitude and tendency. There is an almost linear relation between frequency and current speed, as noticed by Shelley et al. (2005) for a true cantilevered plate. The model reproduces this relation, but get a slightly different slope. The critical velocity is a little bit underestimated.

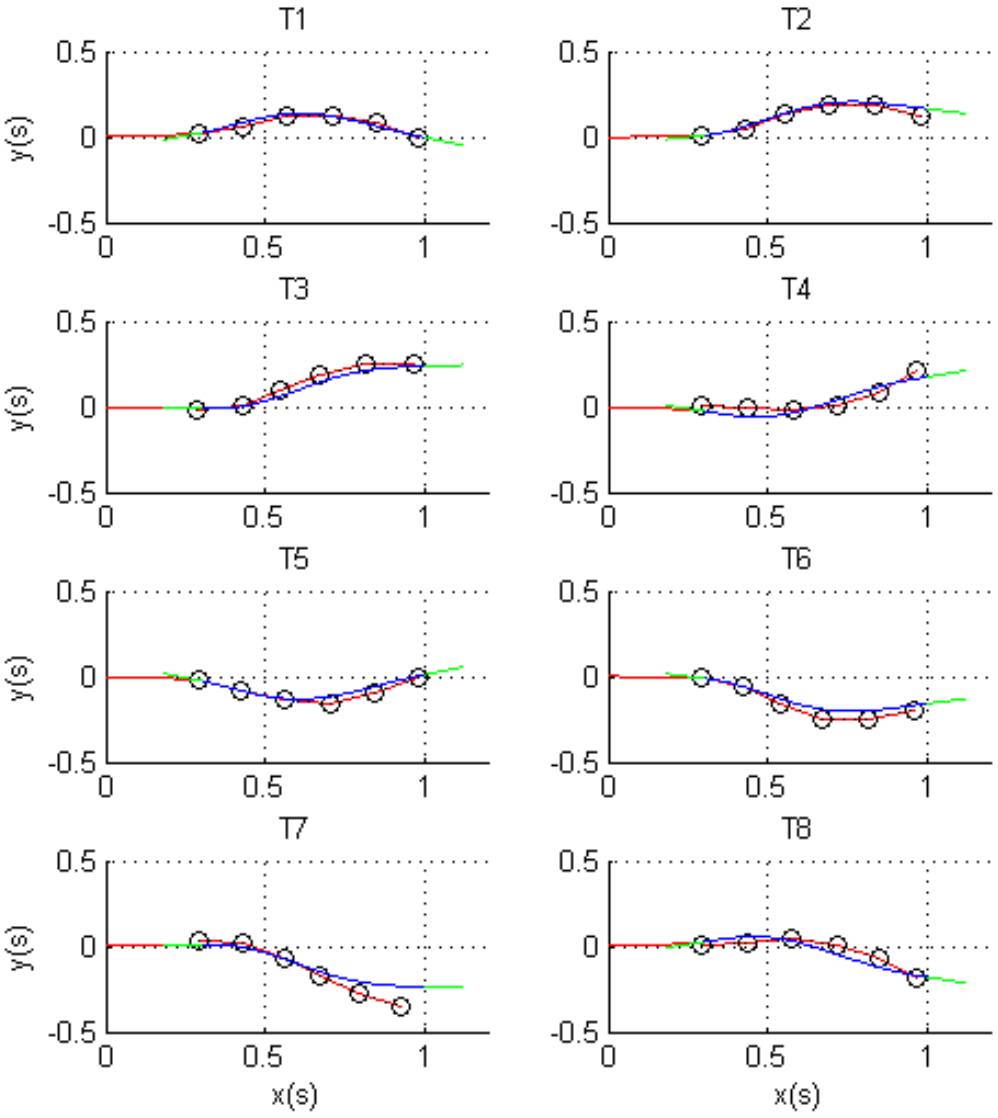

Figure 8: Experiment and analytical model snapshots for undulation mode comparison for u=9.98 during a motion period. Time of each frame is represented on Fig. 7 Membrane is blue, arm is red and flaps are green. Superimposed in black are shapes measured in experiments for equivalent configuration and time. Circles indicate motion tracking targets' positions.

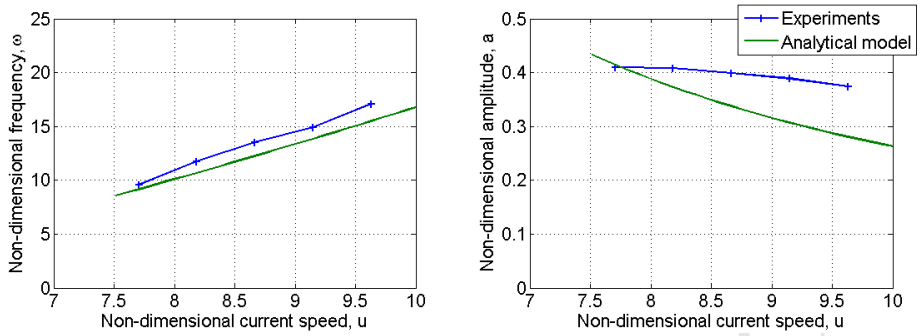

Figure 9: Experimental and analytical model comparison of motion frequency (left) and amplitude at downstream extremity (right). $L^{eq}_{bras} = 0.140L_0$; $L_{flap} = 0.146L_0$; $\beta = 0.991$; $C_d = 0.6$; $\mu = 0.0292$

Results of maximum amplitude for different current velocities are presented on the right of Fig. 9. It shows that the model gives approximate results for absolute amplitude, but with the right tendency. Indeed, it tends to decrease when the flow speed increases. This is an effect of the cables, because it is opposite to the tendency one can find in the literature for true cantilever plate in Eloy et al. (2011) or Tang (2007), for example. The amplitude's values and slope are however very different, which results in increasing errors for the highest values of flow speed. It could come from fluid and solid non-linear dynamics that are not taken into account in the model.

This model is based on assumptions about boundary conditions and cable compression force (both about direction and time variation). The fluid dynamic has been simplified: turbulence and boudary layer, vortex shedding and wake effects on the interacting flow have been neglected. Therefore it should be used for low fluid velocity and small membrane deflection. The 2D hypothesis does not allow to take into account the edge effects. It is limited to one unstable mode, and does not take into account higher frequencies when there should be coupled mode flutter. Therefore, the membrane should be rigid enough and damped enough to stabilize those modes. The elongated body theory is used and no gravity was implemented, so the simulated membrane should be with small thickness and density close to the fluid one. The model can still be used for parametric studies: in the next section the effect of buckling cables will be studied, then there will be a focus on Power Take-Off through damping formulation.

4. Buckling cables effects on the undulating membrane

The parametric study presented in this chapter will focus on the most innovative aspect of this model: the buckling cables, through the parameters Γ and ι. They respectively represent the cable's effect on frequency/stability and motion amplitude of the membrane. The damping factor will be presented on section 5. The mass ratio influence study is not relevant here because for an undulating tidal energy converter the fluid added mass is so heavy in comparison with the linear membrane mass that the mass ratio β will always be close to 1. Its formulation differs from what is usually used in flow-induced vibration literature but is really convenient to solve the system's equation (Eq. 10 & 11).

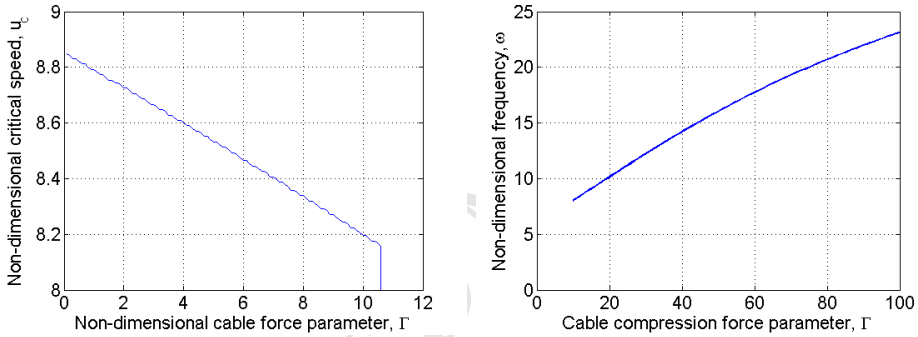

Figure 10: On the left: Effect of compression force on critical speed. On the right: Influence of cable length on motion amplitude. $L^{eq}_{bras} = 0.140L_0$; $L_{flap} = 0.146L_0$; $\beta = 0.991$; $C_d = 0.6$; $\mu = 0.0292$.

Fig. 10 shows on the left the critical current speed as a function of compression force parameter Γ. It is important to underline that during experiments, when we reduce the compression cable length, the critical velocity tends to raise. However, it is not in contradiction with the results of this model because Γ does not change in regards to the compression length. Indeed, when a lateral displacement is imposed on buckling, the compression force increases very little above its critical value (Arnoult (2010)). Instead, the reduction of the cable length increases the eigenmodes and tends to stabilize the structure. We should also notice that when using a similar model, there should be a critical Γ_c above which the system is always unstable even for $u = 0$, as in the garden-hose instability (Doare and De Langre (2002)). Here, $\Gamma_c = 10.6$.

The influence of the cable compression force coefficient Γ on undulation frequency is plotted in the right of Fig. 11. It shows that frequency is strongly linked with this parameter. An augmentation of the compression force implies an increase in frequency. It can be counter-intuitive but is indeed in accordance with Dowell (1982). The membrane downstream's end is most of the time in the same direction as its motion (Fig. 8), then Γ accelerates the membrane's downstream motion. However when $y(L)$ reaches an extrema, the tip force is on opposite direction and acts on motion inversion. Therefore it increases undulation frequency. Fig. 10 highlights the benefits of a buckled membrane in this case for which the unstability is the objective: the compression force reduces critical speed and increases frequency.

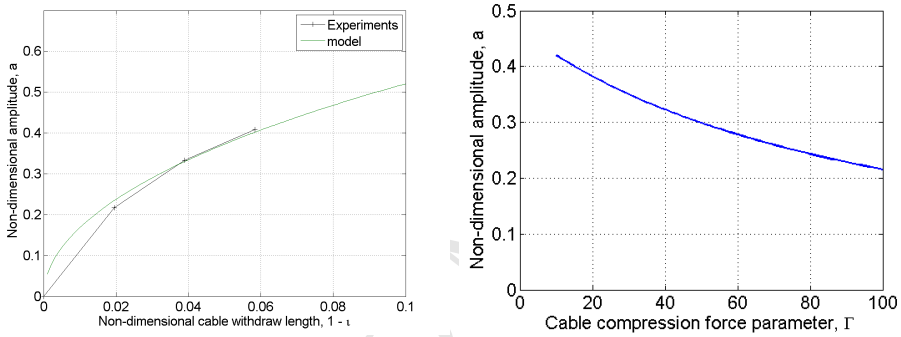

Figure 11: Influence of Γ on motion frequency (on the left) and amplitude (on the right). $L^{eq}_{bras} = 0.140L_0$; $L_{flap} = 0.146L_0$; $\beta = 0.991$; $u = 8.19$; $C_d = 0.6$ and $\mu = 0.0292$.

The results of motion amplitude as a function of cable withdraw length obtained by Eq. 26 represents well the tendency observed in the experiments, as indicated by the graph in the left of Fig. 11. A quadratic relationship exists between a and $(1 - \iota)$, as demonstrated in (Träsch et al (2017)) for static and dynamic buckled membrane in fluid flow. The right graph of Fig. 11 shows a decrease of motion amplitude as the compression force parameter Γ increases. Indeed, Γ accelerates motion inversion and enhances membrane curvature, which tends to reduce maximum amplitude as shown by Eq. 26.

5. Extrapolation of power take-off

In this section we extrapolate the behaviour of the membrane when undergoing power take-off (PTO). It is a theoretical investigation to forecast the effects of power extraction, here considered equivalent as viscous material dissipation. There are many ways to extract energy from an undulating device. The one chosen here could represent conversion by piezoelectric materials (Singh et al. (2012b)). Power estimates are calculated by Eq. 27, in function of D' (see Eq. 9). $p = \frac{P}{0.5\rho_f L_a A U^3}$ is the non-dimensional collected power, based on the flow power across the frontal area swept by the membrane ($L_a \times A$).

$$P = \frac{1}{\mathcal{T}} \int_0^{\mathcal{T}} \int_{s_{arms}^{eq}}^1 D' \times (\dot{y}'')^2 \mathrm{d}s\mathrm{d}t \tag{27}$$

Furthermore, results of frequency, amplitude and critical speed are presented and interpreted as a function of homogeneous internal damping.

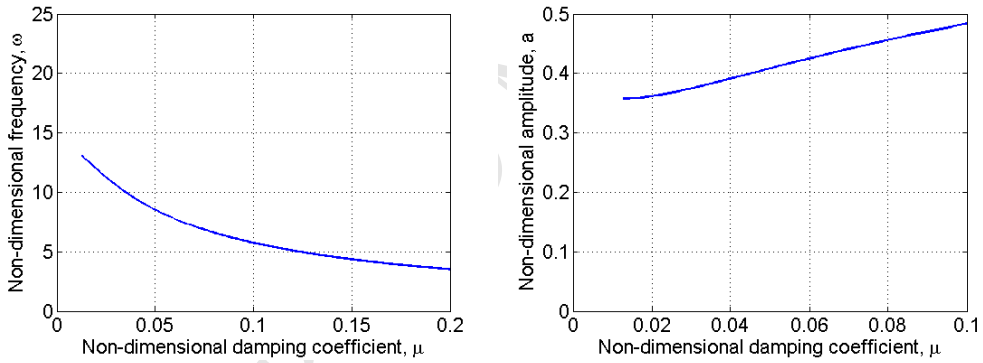

Figure 12: Effect of damping on motion frequency (on the left) and amplitude (on the right). $L_{bras}^{eq} = 0.140L_0$; $L_{flap} = 0.146L_0$; $\Gamma = 22.6$; $\beta = 0.991$; $u = 8.19$; $C_d = 0.6$.

The effect of more damping as a simulation of power take-off is displayed on Fig. 12 and 13. We can see a powerful decrease in frequency and increase in amplitude, caused by a reduction of the flutter mode. However, the higher the damping coefficient is, the less effect its variations will have on the system. Frequency should converge toward 0 and amplitude is limited by membrane's length. Damping has an effect that seems opposite to Γ. This last parameter being set by the device's properties, there must be an optimal μ maximizing collected power.

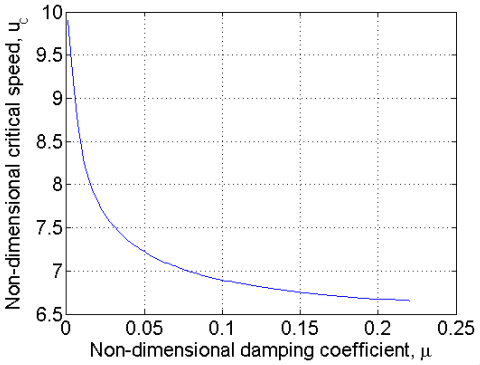

Figure 13: Effect of damping on critical velocity. $L^{eq}_{bras} = 0.140L_0$; $L_{flap} = 0.146L_0$; $\Gamma = 22.6$; $\beta = 0.991$; $C_d = 0.6$.

Another effect of damping is its destabilizing effect for lower modes, as can be noticed on Fig. 13 and Fig. 14. Thus damping lowers critical speed, which is not intuitive but was noticed by other authors for similar systems (Païdoussis (1998), Singh et al. (2012a)). According to Semler (1991), damping causes a phase shift between fluid pressure and solid acceleration, increasing the work done by one on the other and thus their interaction, leading to destabilization. This tendency depends strongly on other parameters, such as the mass ratio, β.

Fig. 14 represents the imaginary part of the eigenfrequencies for different values of the damping coefficient. We can notice that in this configuration it stabilizes higher modes and destabilize the lower ones. Indeed unstable modes occur when $\Im(\omega) < 0$. This can be favourable because it lowers cricital velocity u_c and avoids parasite modes.

Now that we verified the model validity and investigated on buckling cables and PTO effects, we can use this analytical model to draft some power collecting strategies.

Fig. 15 presents the non-dimensional power as a function of damping coefficient for different current speeds. We can notice the existence of an optimal damping coefficient for which the collected power is maximum. This optimal coefficient is function of current speed, which means that the ability to regulate this coefficient dynamically according to the incident fluid velocity would be an asset. In the studied cases, the optimal damping coefficient is smaller when the current is faster. This is not intuitive and could be explained by the fact that the power scales with the damping coefficient but

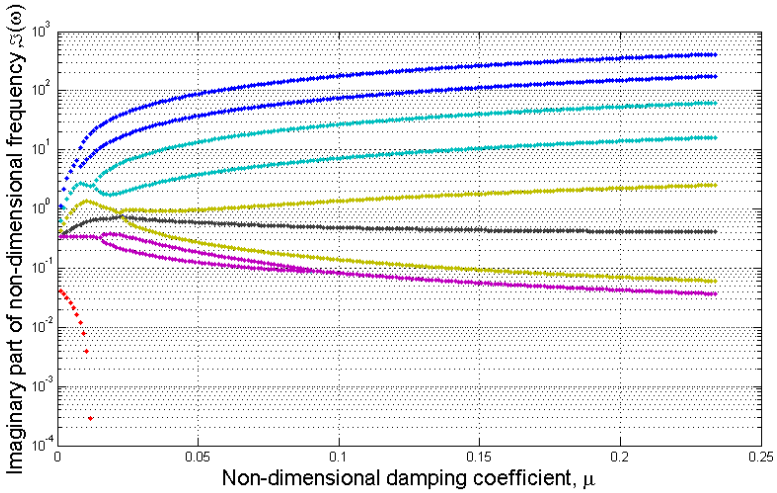

Figure 14: Effect of damping on modes stability. black: 1^{st} mode, red: 2^{nd} mode, purple: 3^{th} mode, yellow: 4^{th} mode, cyan: 5^{th} mode, blue: 6^{th} mode. $L^{eq}_{bras} = 0.140L_0$; $L_{flap} = 0.146L_0$; $\Gamma = 22.6$; $\beta = 0.991$; $u = 8.19$; $C_d = 0.6$.

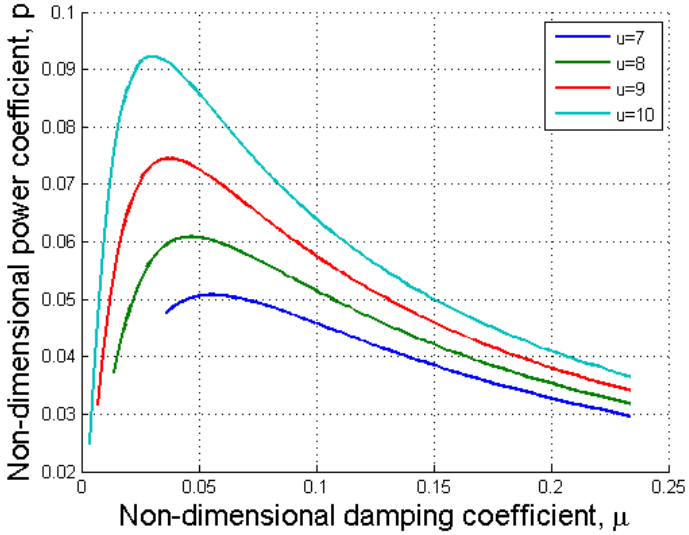

Figure 15: Effect of damping on collected power. $L^{eq}_{bras} = 0.140L_0$; $L_{flap} = 0.146L_0$; $\Gamma = 22.6$; $\beta = 0.991$; $u = 8.19$; $C_d = 0.6$.

with the square of the local deformation speed (Eq. 27). Therefore it is interesting to decrease damping rate in order to have a faster movement, even in configurations where the membrane could be more damped.

However, the increasing error on amplitude estimation (Fig. 9) due to non linear effects may also impact strongly this result.

6. Conclusions and perspectives

In this article we have presented a simple linear analytical model of an undulating tidal energy converter. We used the elongated body theory (Lighthill (1960)) with an approximation of added mass for wide flags (Manela and Howe (2009)). The membrane was modelled using Euler beam theory with Kelvin-Voigt damping. The other elements (flaps, arms, compression cables) where represented by basic physics formulation such as buckling critical load for the cables tension and thin hydrofoil theory for the flaps. The set of ordinary differential equations has been resolved with a method from Païdoussis (1998). Undulating mode, frequency, amplitude and critical speed results are close enough to experimental results to validate the model for its application at low flow speed. The significant role of buckling cables has been underlined thanks to its simplified formulation as compression force and its major impact on undulation amplitude. To represents the power take off system, we used material internal damping. We confirmed that for a given set of parameters, there is an optimal damping coefficient for which the collected power is maximum. This optimal damping coefficient varies with the fluid velocity. The model highlights the main parameters' influence such as compression force Γ, cable length ι and material damping μ. It shall be very usefull for optimization schemes because of its quick computation.

This model is a first step to evaluate the feasability of an analytical model to represent the motion of an undulating membrane tidal energy converter. However, next model versions should differ in the PTO representation, as the conversion system for undulating membrane tidal energy converter will be based on linear actuator (Deporte et al. (2015)). Improvements could make the model more precise considering non-linearities in membrane deflection (Yadakin et al. (2001)) and cable compression force. It should minimize errors and would help us get rid of most impacting hypotheses. Another fluid model, for example based on discrete vortex method with wake implementation should also greatly improve the description of the system dynamics (Tang (2007)). The model could also represent the third dimension to

evaluate the importance of aspect ratio. But what could be gained in precision would be lost in computation time. A good compromise has to be found considering that this model has been developed to be used for multi-parameters optimization.

References

J-B. Drevet. *http://www.eel-energy.fr/en/eel-tidal-energy-convertor/* 19^{th} may 2016.

S. Alben. The flapping-flag instability as a nonlinear eigenvalue problem. *Physics of fluids*, 2008.

M. Argentina and L. Mahadevan. Fluid-flow-induced flutter of a flag. In *Proceedings of the National Academy of Sciences*, 2005.

E. Arnoult. Mécanique des solides déformables. Practical lecture : Buckling study, 2010.

H. Boye, E. Caquot, P. Clement, L. De La Cochetiere, and J.-M. Nataf. Rapport de la mission detude sur les energies marines renouvelables. Technical Report N 2013 / 008693-01 / CGEDD.

R. Coene. Flutter of slender bodies under axial stress. Technical report, Delft University of Technology, 1988.

A.H. Day, A. Babarit, A. Fontaine, Y-P. He, M. Kraskowski, M. Murai, I. Penesis, F. Salvatore, H-K. Shin. Hydrodynamic modelling of marine renewable energy devices: A state of the art review. Ocean Engineering, 2015.

A. Déporte, M. Trasch, G. Germain, A. Artaux, J-B. Drevet, and P. Davies. Three complementary approaches for the development of a flexible membrane tidal energy converter: analytical, experimental and numerical. *European Wave and Tidal Energy Conference*, 2015.

O. Doare and E.l De Langre. The flow-induced instability of long hanging pipes. *European Journal of Mechanics A/Solids*, 21:857–867, February 2002.

O. Doare, M. Sauzade, and C. Eloy. Flutter of an elastic plate in a channel flow: Confinement and finite-size effects. *Journal of Fluids and Structures*, 27(1):76–88, January 2011.

O. Doare and S. Michelin. Piezoelectric coupling in energy-harvesting fluttering flexible plates: linear stability analysis and conversion efficiency. *Journal of Fluids and Structures*, 27(8):1357–1375, November 2011.

E. H. Dowell. Flutter of a bukled plate as an example of chaotic motion of deterministic autonomous system. *Journal of Sound and Vibration*, 85:333–344, 1982.

C. Eloy, C. Souilliez, and L. Schouveiler. Flutter of a rectangular plate. *Journal of Fluids and Structures*, 23(6):904–919, 2007.

C. Eloy, N. Kofman, and L. Shouveiler. The origin of hysteresis in the flag instability. *Journal of Fluid Mechanics*, pages 1–10, 2011.

C. Grouthier, S. Michelin, R. Bourguet, Y. Modarres-Sadeghi, and E. de Langre. On the efficiency of energy collecting using vortex-induced vibrations of cables. *Journal of Fluids and Structures*, 49:427–440, August 2014.

C.Q. Guo and M. P. Paidoussis. Stability of rectangular plates with Free side-edges in two-dimensional inviscid channel flow. *Journal of applied Mechanics*, 67:171–176, 2000.

R.M. Howell, A.D. Lucey, P.W. Carpenter, and M.W. Pitman. Interaction between a cantilevered-free flexible plate and ideal flow. *Journal of Fluids and Structures*, 2008.

L. Huang. Flutter of cantilevered plates in axial flow. *Journal of Fluids and Structures*, 9:127–147, 1995.

T. Kinsey, G. Dumas, G. Lalande, J. Ruel, A. Mehut, P. Viarouge, J. Lemay, and Y. Jean. Prototype testing of a hydrokinetic turbine based on oscillating hydrofoils. *Renewable Energy*, 36(6):1710–1718, June 2011.

A. Kornecki, E.H. Dowell, and J. O'Brien. On the areolastic instability of two-dimenional panels in uniform incompressible flow. *Journal of Sound and Vibration*, 47, 1976.

J.H. Lee and M.M. Bernitsas. High-damping, high-Reynolds VIV tests for energy harnessing using the VIVACE converter. *Ocean Engineering*. 38(16):16971712, November 2011.

C. Lemaitre, P. Hemon, and E. De Langre. Instability of a long ribbon hanging in axial air flow. *Journal of Fluids and Structures*, 20:913–925, 2005.

M. J. Lighthill. Note on the swimming of slender fish. *Journal of Fluid Mechanics*, 9:305–317, 1960.

A. Manela and M.S. S Howe. On the stability and sound of an unforced flag. *Journal of Sound and Vibration*, 321(3-5):994–1006, April 2009.

P. M. Moretti. Tension in fluttering flags *Journal of Acoustics and Vibrations*. pages 1-12, 2003

P. M. Moretti. Flag flutter amplitudes. In *Flow induced vibrations*, 2004.

M. T. Morris-Thomas and S. Steen. Experiments on the stability and drag of a flexible sheet under in-plane tension in uniform flow. *Journal of Fluids and Structures*, 25(5):29, July 2009.

M.P. Païdoussis. *Fluid-structure interactions : Slender structures ans axial flow. Vol1.* Academic press edition, 1998.

M. Pineirua, O. Doaré, and S. Michelin. Influence and optimization of the electrodes position in a piezoelectric energy harvesting flag. *Journal of Sound and Vibration*, 346:200–215, January 2015.

C. Semler. *Nonlinear dynamics and chaos of a pipe conveying fluid*. PhD thesis, McGill University, 1991.

M. Shelley, N. Vandenberghe, and J. Zhang. Heavy flags undergo spontaneous oscillations in flowing water. *Physical Review Letters*, 94:094302, March 2005.

M. J. Shelley and J. Zhang. Flapping and Bending Bodies Interacting with Fluid Flows. *Annual Review of Fluid Mechanics*, 43(1):449–465, January 2011.

S. Shi, T.H. New, and Y. Liu. Flapping dynamics of a low aspect-ratio energy-harvesting membrane immersed in a square cylinder wake. *Experimental Thermal and Fluid Science*, 46:151–161, April 2013.

K. Singh, S. Michelin, and E. de Langre. Energy harvesting from axial fluid-elastic instabilities of a cylinder. *Journal of Fluids and Structures*, 30:159–172, April 2012.

K. Singh, S. Michelin, and E. De Langre. The effect of non-uniform damping on flutter in axial flow and energy-harvesting strategies. *Proceedings of the Royal Society A: Mathematical, Physical and Engineering Sciences*, 468(2147):3620–3635, 2012.

L. Tang. *The dynamics of two-dimensional cantilevered flexible plates in axial flow and a new energy-harvesting concept*. PhD thesis, McGill University, 2007.

G.W. Taylor, J.R. Burns, S.a. Kammann, W.B. Powers, and T.R. Welsh. The Energy Harvesting Eel: a small subsurface ocean/river power generator. *IEEE Journal of Oceanic Engineering*, 26(4):539–547, 2001.

I. P. L. Tecnomare SpA. The exploitation of tidal marine currents. Technical Report EUR16683EN.

M. Träsch, A. Déporte, J.-B. Drevet and G. Germain Impact of cables withdraw length on the dynamics of an undulating membrane tidal energy converter *European Wave and Tidal Energy Conference*, Cork, 2017.

M. Träsch, A. Déporte, S. Delacroix, B. Gaurier, G. Germain and J.-B. Drevet Power estimates of an undulating membrane tidal energy converter *Ocean Engineering*, 2018.

Y. Watanabe, K. Isogai, S. Suzuki, and M. Sugihara. A Theoretical Study of Paper Flutter. *Journal of Fluids and Structures*, 2001.

Y. Watanabe, S. Suzuki, M. Sugihara, and Y. Sueoka. An Experimental Study of Paper Flutter. *Journal of Fluids and Structures*, 16(4):529–542, May 2002.

Q. Xiao and Q. Zhu. A review on flow energy harvesters based on flapping foils. *Journal of Fluids and Structures*, 46:174–191, April 2014.

Y. Yadakin, V. Tenetov, and D. Levin. The flow-induced vibration of a flexible strip hanging vertically in a parallel flow. Part 1: Temporal aeoelastic instability. *Journal of fluids and Structures*, 15:1167–1185, 2001.